An intrinsic source of radial electric field and edge flows in tokamaks

2009 Nucl. Fusion 49 065001

(http://iopscience.iop.org/0029-5515/49/6/065001)

IOP Publishing and International Atomic Energy Agency Nuclear Fusion
Nucl. Fusion **49** (2009) 065001 (6pp) doi:10.1088/0029-5515/49/6/065001

An intrinsic source of radial electric field and edge flows in tokamaks

A.Y. Aydemir

Institute for Fusion Studies, The University of Texas at Austin, Austin, TX 78712, USA

E-mail: aydemir@mail.utexas.edu

Received 5 January 2009, accepted for publication 25 March 2009
Published 30 April 2009
Online at stacks.iop.org/NF/49/065001

Abstract
We propose a new mechanism for radial electric fields and edge flows in tokamaks that will also serve as an intrinsic momentum source in systems without an up–down symmetry. An essential feature of toroidal plasmas is that charge-dependent ∇B and curvature drifts would lead to a vertical polarization of the discharge if it were not for the Pfirsch–Schlüter currents that neutralize the resulting charge separation. However, in the presence of collisions, there is a residual vertical electric field that drives an $\boldsymbol{E}\times\boldsymbol{B}$ flow in the direction of increasing major radius, regardless of the orientation of the fields and currents. This flow is excluded from the hot core and is localized to the more collisional edge plasma. It has many features in common with the edge flows observed in tokamaks such as C-Mod. In an up–down symmetric geometry it carries no net toroidal angular momentum; however, its viscous interaction with asymmetric boundaries leads to a net momentum input to the plasma. Both this momentum input, and the residual vertical electric field, the source of these flows, may play an important role in the ∇B direction-dependence of the power threshold for the L–H transition.

PACS numbers: 52.30.Cv, 52.55.Fa, 52.65.Kj

(Some figures in this article are in colour only in the electronic version)

1. Introduction

The tokamak edge, loosely defined in this work to be the region extending from the foot of the pedestal inside the separatrix to the inner scrape-off layer (SOL), exhibits flows documented on nearly all tokamaks [1–3]. While there are undoubtably a number of different sources for these flows, here we present a fundamental mechanism that does not seem to have drawn much attention to date.

An unavoidable feature of toroidal confinement is that charge-dependent ∇B and curvature drifts, in the absence of neutralizing flows, would set up a vertical electric field, and the resulting $\boldsymbol{E}\times\boldsymbol{B}$ drift would lead to an immediate loss of confinement. Of course with finite rotational transform, this vertical polarization and the associated electric field tend to be short-circuited by parallel currents. In a fluid model, the ∇B-dependent drifts do not appear explicitly but are subsumed by the diamagnetic current, $\boldsymbol{J}_\perp = \boldsymbol{B}\times\nabla p/B^2$, while the Pfirsch–Schlüter currents, $J_{\rm PS}$, ensure charge continuity by playing the role of a neutralizing charge flow, $\nabla\cdot(\boldsymbol{J}_\perp + J_{\rm PS}\boldsymbol{B}/B) = 0$.

With collisions, this idealized picture is altered somewhat. Although the charge continuity condition above is still satisfied in steady state, both the diamagnetic and parallel components of the current are modified, leaving behind a residual electric field that still drives an outward (in the direction of increasing major radius, $\hat{\boldsymbol{R}}$) $\boldsymbol{E}\times\boldsymbol{B}$-flow. However, since the hot core is essentially collisionless in modern tokamaks, this flow is confined to the more collisional edge plasma. In fact, as we will see below, higher collisionality and the presence of a pressure pedestal both play a role in this localization.

The residual electric field that results from finite collisionality points upward for a 'normal' configuration of the toroidal field and current (they are both clockwise as seen from above) and reverses direction with the toroidal field, as seen in figure 1. In the usual toroidal coordinate system (r,θ,ζ), where θ is measured from the outboard mid-plane, and ignoring any other contributions for the moment, components of the electric field are $E_r = E_v\sin\theta$, $E_\theta = E_v\cos\theta$, which leads to the following poloidal flow:

$$u_r = E_v B_\zeta\cos\theta/B^2, \tag{1}$$

$$u_\theta = -E_v B_\zeta\sin\theta/B^2. \tag{2}$$

For the up–down symmetric system shown in figure 1, the flow pattern is an exact dipole with two counter-rotating vortices localized to the edge. As is obvious from the physics behind them, these poloidal flows are always in the direction shown. The electric field E_v reverses with the toroidal field

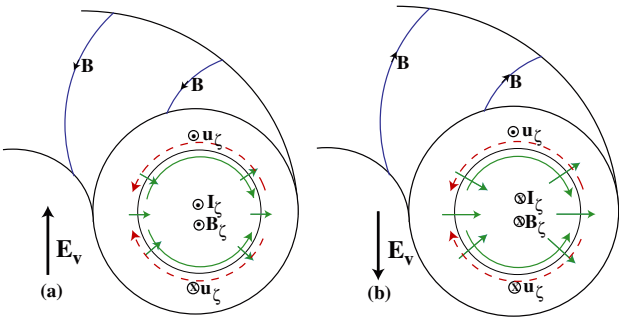

Figure 1. A schematic description of the flows discussed here. The solid arrows represent the flows driven by the residual electric field due to polarization charges. The dashed arrows outside the separatrix (the inner solid circle) are the return flows in the SOL. (*a*) With the toroidal field and current in the 'normal' configuration. (*b*) With the magnetic fields and currents reversed. Note that the electric field reverses with the ∇B-drifts, but the toroidal and poloidal flows, both inside and outside, do not change direction.

B_ζ but the poloidal flows retain their sign. We disagree with Simakov *et al* [4] on this point; this issue is briefly re-examined in appendix A. Reversal of the toroidal current has no effect on (u_r, u_θ) either. The toroidal component of the flow is given by

$$u_\zeta \simeq E_r B_\theta / B^2 = E_v B_\theta \sin\theta / B^2. \tag{3}$$

Note that u_ζ is anti-symmetric with respect to the mid-plane in the up–down symmetric geometry of figure 1; thus, there is no net toroidal angular momentum contribution. Unlike the poloidal flows, however, the toroidal flow changes sign with the toroidal field (which reverses E_v), and the toroidal current (which reverses B_θ), but not when both are reversed simultaneously, as in figure 1. A more complete discussion of the symmetries of these flows can be found in [5, 6].

The direction of the flows outside the separatrix are determined by a global mass conservation requirement. Without the return flows, whose poloidal projection is indicated by dashed lines in figure 1, one would get an accumulation of material at the outside mid-plane. Thus, these are essentially parallel flows driven by a pressure gradient. With $\boldsymbol{u} \simeq u_\parallel \boldsymbol{B}/B$, in the upper half plane $u_\theta > 0$ requires a positive $u_\parallel$, which also leads to $u_\zeta > 0$. Note that although the poloidal component of the flow is anti-symmetric with respect to the separatrix, the toroidal component is symmetric, having the same sign on both sides. At the bottom, the parallel flow reverses, $u_\parallel < 0$, leading to $u_\theta < 0, u_\zeta < 0$.

In this introduction, we gave a physics overview of the flows and their general properties. In the following sections, we present a more quantitative picture and discuss numerical calculations in various magnetic topologies while making comparisons with experiments where appropriate.

2. A more quantitative model of the flows

Assuming axisymmetry and working in a flux coordinate system (ψ, θ, ζ), we can write the general equilibrium current in the form

$$\mu_0 \boldsymbol{J} = \mu_0 R^2 p' \nabla\zeta + F' \boldsymbol{B}, \tag{4}$$

where we let $\boldsymbol{B} = \nabla\psi \times \nabla\zeta + F\nabla\zeta$, $\psi \equiv R^2(\boldsymbol{A}\cdot\nabla\zeta)$ and $F \equiv R^2(\boldsymbol{B}\cdot\nabla\zeta)$. Here we also assume that the flow velocities are sub-sonic so that the Grad–Shafranov equation, $-\Delta^\star\psi \equiv -R^2\nabla\cdot((1/R^2)\nabla\psi) = \mu_0 R^2 p' + FF'$ still holds ($p' \equiv \mathrm{d}p/\mathrm{d}\psi$, $F' \equiv \mathrm{d}F/\mathrm{d}\psi$). Note that we identify the coordinate ζ with the usual toroidal angle so that $|\nabla\zeta|^2 = 1/R^2$. Recall also that consistency requirement leads to the following relationship among p', F' and the parallel current:

$$F' = \mu_0 \frac{\langle J_\parallel B\rangle - Fp'}{\langle B^2\rangle}, \tag{5}$$

where the brackets denote the flux-surface average

$$\langle A\rangle \equiv \oint A\mathcal{J}\,\mathrm{d}\theta \left(\oint \mathcal{J}\,\mathrm{d}\theta\right)^{-1} = \oint AR^2\,\mathrm{d}\theta \left(\oint R^2\,\mathrm{d}\theta\right)^{-1}, \tag{6}$$

and the Jacobian $\mathcal{J} = 1/\nabla\psi\cdot\nabla\theta\times\nabla\zeta = -1/\boldsymbol{B}\cdot\nabla\theta = -q(\psi)R^2/F(\psi)$, where the safety factor $q(\psi) = (\boldsymbol{B}\cdot\nabla\zeta)/(\boldsymbol{B}\cdot\nabla\theta)$. It is useful to also define the usual average of A on a flux surface:

$$\bar{A} \equiv \frac{1}{2\pi}\oint A\,\mathrm{d}\theta = \frac{\langle A/R^2\rangle}{\langle 1/R^2\rangle}. \tag{7}$$

With these preliminaries we are ready to have a more quantitative look at the $\boldsymbol{E}\times\boldsymbol{B}$ flows at the edge. Since the vertical electric field discussed in the previous section arises from collisional effects acting on the parallel (mostly Pfirsch–Schlüter) currents, we examine the parallel electric field, starting with the simple Ohm's law

$$\boldsymbol{E} = -\nabla\phi + \nabla(V_l\zeta) = -\boldsymbol{u}\times\boldsymbol{B} + \eta\boldsymbol{J}, \tag{8}$$

where V_l is the loop voltage. Then $E_\parallel B = \eta J_\parallel B$ leads to

$$E_\theta = -\frac{\partial\phi}{\partial\theta} = \frac{\mathcal{J}F}{R^2}V_l - \eta\mathcal{J}J_\parallel B. \tag{9}$$

Note that subscripts (superscripts) denote covariant (contravariant) components of vectors; thus $E_\theta = \boldsymbol{E}\cdot(\partial\boldsymbol{r}/\partial\theta)$. Using equations (4) and (5), and noting that for Ohmic current we have (after using $\langle\boldsymbol{B}\cdot\nabla\phi\rangle = 0$) in the equation above

$$\langle J_\parallel B\rangle = \frac{V_l F}{\eta}\langle 1/R^2\rangle, \tag{10}$$

we get

$$E_\theta = -qV_l\left(1 - R^2\langle 1/R^2\rangle\frac{B^2}{\langle B^2\rangle}\right) + \eta q R^2 p'\left(1 - \frac{B^2}{\langle B^2\rangle}\right), \tag{11}$$

where we assumed $\eta = \eta(\psi)$. Using equation (7), one can easily show that

$$\oint E_\theta\,\mathrm{d}\theta = 0, \tag{12}$$

as expected. In fact, both terms on the right-hand side of equation (11) vanish independently. The pressure-gradient (Pfirsch–Schlüter) term dominates and determines the sign of E_θ. With our sign convention for ψ, we have $p' > 0$ for radially decreasing pressure profiles. Also $(1 - B^2/\langle B^2\rangle)$ is negative (positive) on the high (low) field side of the tokamak. Thus $E_\theta < 0$ on the high-field side and positive elsewhere, in agreement with the simple analysis of the previous section, where we had $E_\theta = E_v\cos\theta$. Note also qV_l

and qp' are invariant under $\psi \to -\psi$ (reversal of the plasma current), but both flip sign with $F \to -F$ (reversal of the toroidal field), as expected.

An alternative and more useful expression for the poloidal electric field can be obtained by eliminating V_l in favour of F' to obtain

$$E_\theta = \eta q \left[p'(R^2 - \overline{R^2}) + \frac{F'}{\mu_0 F}(|\nabla\psi|^2 - \overline{|\nabla\psi|^2}) \right], \tag{13}$$

which leads to the same conclusions regarding symmetry and sign of the poloidal electric field. We can use equation (13) to find an approximate expression for the radial electric field near the separatrix. Again concentrating on the pressure-gradient term and integrating along a flux surface close to $\psi = \psi_\mathrm{sep}$, we have

$$\phi(\psi,\theta) \simeq -\eta q p' \left(\int_0^\theta R^2 \,\mathrm{d}\tilde{\theta} - \frac{\theta}{2\pi} \oint R^2 \,\mathrm{d}\tilde{\theta} \right), \tag{14}$$

where we set the integration constant $\phi(\psi, 0)$ to zero. The largest radial variation in $\phi(\psi,\theta)$ near the separatrix comes from the (ηq) term since both the resistivity and safety factor increase rapidly as we approach the separatrix; thus,

$$E_\psi = -\frac{\partial\phi}{\partial\psi} \simeq \frac{\partial(\eta q)}{\partial\psi} p' f(\psi,\theta),$$
$$f(\psi,\theta) \equiv \int_0^\theta R^2 \,\mathrm{d}\tilde{\theta} - \frac{\theta}{2\pi} \oint R^2 \,\mathrm{d}\tilde{\theta}. \tag{15}$$

For an arbitrary flux surface parametrically defined by $(R = R(\psi,\theta), Z = Z(\psi,\theta))$, assume that $\partial R/\partial\theta = 0$ at $\theta = 0, \pi$, and that $R(\psi, 0) = R_\mathrm{max}$, $R(\psi,\pi) = R_\mathrm{min}$. Then it is easy to see that

$$f(\psi,\theta) > 0 \qquad \text{for } 0 \leqslant \theta < \pi$$

and

$$f(\psi,\theta) < 0 \qquad \text{for } \pi \leqslant \theta < 2\pi. \tag{16}$$

(Validity of these inequalities under general conditions is shown in appendix B.) Again recalling our sign convention for ψ that makes $\nabla\psi \sim -\nabla r$, $p' > 0$, and $(\eta q)' < 0$ near the separatrix (fields are in the 'normal' configuration of figure 1(*a*)), we have

$E_\psi < 0$ $(E_r > 0)$ in the upper half plane

and

$E_\psi > 0$ $(E_r < 0)$ in the lower half plane. (17)

This result is also in agreement with the analysis of the previous section where we had $E_r = E_v \sin\theta$. Note that $E_\psi = \boldsymbol{E}\cdot(\partial\boldsymbol{r}/\partial\psi)$ reverses sign with $\psi \to -\psi$, but only because $(\partial\boldsymbol{r}/\partial\psi)$ reverses direction, not because of a change in $\boldsymbol{E}$ itself. It changes sign with $F \to -F$ also, but now this represents an actual change in the vector $\boldsymbol{E}$. In other words, $\boldsymbol{E}$ reverses sign when the toroidal field is reversed, as expected from an electric field due to non-neutralized polarization charges generated by toroidal drifts, but not when the toroidal current is reversed. Note also the sign of the potential in equation (14) (negative in the upper half plane and positive below) implies an electric field pointing up as in figure 1(*a*) for the plasma current and field configuration shown there.

Above we demonstrated that collisional effects acting on the Pfirsch–Schlüter currents lead to the same electric fields at the edge that were explained with a simpler model in the previous section. And it is clear that the resulting $\boldsymbol{E}\times\boldsymbol{B}$ drift will generate the kind of edge flows discussed there (figure 1). Here we take a more detailed look at the radial flow and demonstrate that it is consistent with our simpler model. Starting with the ψ-component of Ohm's law in equation (8),

$$u^\psi = (\boldsymbol{u}\cdot\nabla\psi) = -\eta\left(R^2 p' + \frac{FF'}{\mu_0}\right) + V_\mathrm{l}, \tag{18}$$

and using equations (5) and (10), we obtain

$$u^\psi = -\eta R^2 p' \left(1 - \frac{F^2}{R^2\langle B^2\rangle}\right) + V_\mathrm{l}\left(1 - \frac{F^2\langle 1/R^2\rangle}{\langle B^2\rangle}\right), \tag{19}$$

or alternatively, after eliminating V_l,

$$u^\psi = -\eta p'(R^2 - \overline{R^2}) + \frac{\eta F'}{\mu_0 F}\overline{|\nabla\psi|^2}, \tag{20}$$

which makes the Pfirsh–Schlüter and classical diffusion contributions to the radial flux clearer. It is helpful to isolate the net radial flux:

$$u_\mathrm{rad} \equiv -u^\psi + \langle u^\psi\rangle = \eta p'(R^2 - \langle R^2\rangle), \tag{21}$$

which shows that there is a net inflow at the inboard and a net outflow at the outboard sides of the torus, in agreement with figure 1 of the previous section.

Making use of the radial electric field in equation (15), and $\boldsymbol{u} \equiv \boldsymbol{u}_\perp = \boldsymbol{E}\times\boldsymbol{B}/B^2 - \eta\nabla p/B^2$, we can show that the poloidal velocity is given by

$$u^\theta \simeq \frac{f(\psi,\theta)F^2}{qR^2B^2} p'(\eta q)' + (V_l - \eta R^2 p')\frac{(\nabla\psi\cdot\nabla\theta)}{R^2B^2}, \tag{22}$$

where the function $f(\psi,\theta)$ defined in equation (15) was shown to be positive (negative) in the upper (lower) half plane. For up–down symmetric systems, the first term on the right-hand side dominates and leads to the anti-symmetric poloidal flows within the separatrix shown in figure 1. In non-symmetric systems, the second term alters this perfect anti-symmetry ($\nabla\psi \to 0$ near the X-point) and leads to a more complex flow pattern, as we will see in the numerical calculations of the next section. Note that u^θ is invariant under the transformations $\psi \to -\psi$, and/or $F \to -F$; in other words, reversal of the toroidal current or toroidal field, individually or together, does not affect this poloidal flow from the inboard side of the torus to the outside.

The amplitude of the net radial flow is proportional to resistivity (equation (21)) and at first glance might be expected to be trivially small. Note, however, the model describes physics around the separatrix (near the bottom of the pedestal), not in the hot core. Secondly, the relevant quantity is the poloidal velocity, which scales as $u_\mathrm{p} \sim (a/\delta)u_\mathrm{rad}$, where a, δ are the minor radius and flow layer width, respectively, with $\delta \sim (\eta q)/(\eta q)'$, and $a/\delta \gg 1$. A more comprehensive look at scaling of these flows with resistivity at the edge can be found in [6].

In the next section results of numerical calculations with our *CTD* code are discussed.

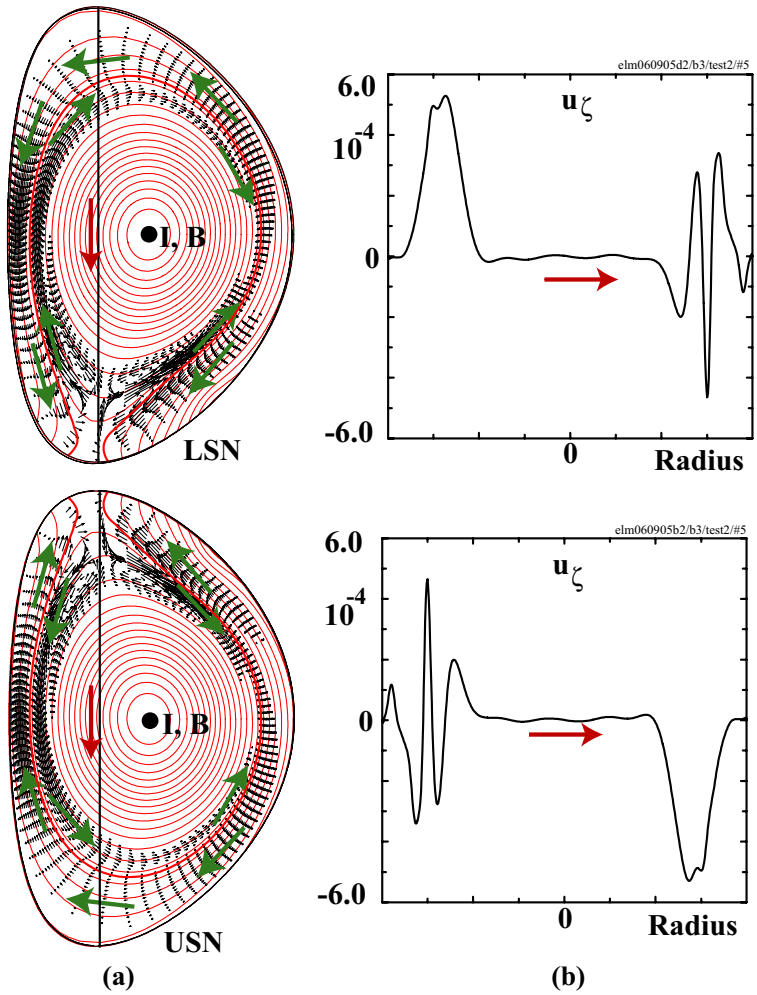

Figure 2. Quasi-steady-state flows generated by the *CTD* code for upper and lower single-null magnetic geometries. Magnetic fields and current are in the 'normal' direction. (*a*) Poloidal projections of the flows, both inside and outside the separatrix. Note that the flows retain their dipole nature (see figure 1), but in these asymmetric geometries, the half of the dipole flow away from the X-point expands at the expense of the other half. In both geometries there are strong flows in the SOL from the low-field to the high-field side and eventually to the X-point. (*b*) Toroidal projection of the flows along a vertical line passing approximately through the centre and connecting the top to the bottom of the device. Here also, the portion near the X-point of the anti-symmetrix flow gets modified and damped through viscous dissipation, resulting in a net momentum input to the plasma.

3. Numerical calculations

The flows discussed above were first observed in our attempts to find quasi-equilibrium states in the presence of various transport processes, such as viscous and resistive dissipation. There were earlier discussions of these states, but not with realistic tokamak profiles and geometries [7, 8]. The calculations use our toroidal magnetohydrodynamic (MHD) code *CTD*. The exact model and some of the relevant details of our calculations can be found in [5, 6] and the references therein.

Quasi-steady state flows found with the *CTD* code for lower-single-null (LSN) and upper-single-null (USN) field geometries are shown in figure 2. Although the perfect dipole pattern of figure 1 is retained for a symmetric double-null configuration (not shown here; see figure 2(*a*) in [6]), the flows are modified in an asymmetric field geometry. However, their dipole character still survives, as seen in figure 2(*a*). Note that, of the two counter-rotating vortices mentioned in the Introduction, the one away from the X-point expands in size at the expense of the other. Part of this larger vortex located in the SOL is seen to connect the low-field side of the torus to the high-field side, and eventually down (or up) to the X-point. In this simple treatment of the divertor region, that flow enters back into the plasma at the X-point, forming the inner half of the vortex that connects the X-point to the outer mid-plane. In figure 2(*b*), toroidal projection of the flows is shown along a vertical line connecting the top to the bottom of the torus approximately through its centre. Although the toroidal velocity is anti-symmetric for an up–down symmetric configuration like a double-null geometry (see figure 1 and equation (3)), that anti-symmetry is broken by an asymmetric field topology, as seen in the figures. Again, the portion of the flow near the X-point gets damped through its viscous interaction with the open field lines. Thus, some of the momentum is transferred to the vessel through the field lines, leaving behind a net momentum input to the plasma. Toroidal momentum transferred to the plasma is

positive for LSN and negative for USN topologies, as seen in figure 2(*b*).

In order to get an estimate of the expected poloidal velocity amplitudes based on these calculations, we use the following parameters, assumed to be typical of C-Mod edge profiles in L-Mode discharges: $B = 5.4\,\mathrm{T}$, $n = 10^{20}\,\mathrm{m}^{-3}$, $T_\mathrm{e} = 100\,\mathrm{eV}$, L (length scale) $= 5 \times 10^{-3}\,\mathrm{m}$, which leads to an Alfvén velocity of $v_\mathrm{A} = 1.18 \times 10^7\,\mathrm{m\,s}^{-1}$, and Alfvén time of $\tau_\mathrm{A} = L/v_\mathrm{A} = 4.25 \times 10^{-10}\,\mathrm{s}$. For the same parameters, the edge resistivity is $\eta = 1.55 \times 10^{-6}\,\Omega\,\mathrm{m}$, where we conservatively assumed $Z = 1$ and $\ln\Lambda = 15$. Thus, the resistive diffusion time $\tau_\mathrm{R} = \mu_0 L^2/\eta = 2.03 \times 10^{-5}\,\mathrm{s}$, and the Lundquist number $S = \tau_\mathrm{R}/\tau_\mathrm{A} = 4.78 \times 10^4$. In figure 3(*a*) of [6], this corresponds to $\eta_0 = 1/S_0 = 2.09 \times 10^{-5} \times 10^{-5} = 2.09 \times 10^{-10}$, which is outside the range of the scaling study of that figure. But it is clear that the expected poloidal velocity (normalized to v_A) is of the order of 10^{-4}, which leads to an approximate poloidal velocity of $V_\mathrm{pol} = 10^3\,\mathrm{m\,s}^{-1}$. However, as stated in the caption for that figure, the average toroidal $\beta = 5 \times 10^{-5}$ in that work, with an edge $\beta = 2\mu_0 p/B^2 \sim 10^{-5}$. The C-Mod parameters above give $p = nkT = 1.6 \times 10^3\,\mathrm{Pa}$ and $\beta = 1.4 \times 10^{-4}$. Although calculations were not done at this particular value of β, both from the theoretical discussions in section 2 and available numerical evidence, we expect V_pol to scale linearly with edge β. Thus, extrapolating to C-Mod conditions, we get $V_\mathrm{pol} \sim 10^4\,\mathrm{m\,s}^{-1}$, which is comparable to the velocities observed in the experiment [2, 11].

Note that SOL flows similar to those shown in figure 2 have also been observed in fluid simulations of NSTX equilibria with flows [9], and two-dimensional particle simulations of SOL flows in USN and LSN divertor configurations [10].

For all field/current directions and magnetic topologies, our results are in qualitative agreement with the experimental observations from C-Mod. For the cases with the field/current in the 'normal' direction, this agreement is readily apparent when the SOL flows in figure 2 are compared with figure 8 in [11], or figure 16 in [2]. For the two cases in [11] where the field and currents are reversed, our results (not shown here) are also in agreement, since the transformation $\boldsymbol{B} \to -\boldsymbol{B}, \boldsymbol{u} \to +\boldsymbol{u}$ is a symmetry of our computational model [5, 6]. In other words, with the magnetic topology fixed in USN or LSN configuration, reversing all currents and fields do not alter the flows in our calculations, in agreement with figure 8 of [11].

4. Radial electric field and its effect on the L–H transition power threshold

The momentum input to the plasma from the SOL flows and its effect on the L–H transition power threshold have been discussed extensively by the C-Mod group (see, for example, [2]). Here, we will simply recall the dynamical origins of these effects in our model and examine its contribution in various field configurations using symmetry arguments.

As already discussed in previous sections, both the E_v-driven flows within the separatrix and the parallel return flows in the SOL have an anti-symmetric toroidal component in up–down symmetric geometries (again, see equation (3)). But in a LSN topology, the lower portion of this toroidal flow is damped with respect to the upper, with the lost momentum being absorbed by the vessel. Since the intact upper portion is positive when the toroidal field is in the 'normal' direction, there will be a net positive momentum input to the plasma. Another important factor that determines the power threshold is the direction of the residual electric field E_v. Recall that the resulting radial electric field within the separatrix is $E_r = E_v \sin\theta$, which is negative approximately below the mid-plane (on the side with the X-point) and positive above (see also equation (15) and the associated discussion there). Assuming that this particular direction of E_r makes the L–H transition easier with a net addition to, for example, the ion-orbit loss generated radial electric field [12], and using this LSN with the fields in the 'normal' direction as the base case, we can make the following predictions based on symmetry arguments [5, 6].

- Reversal of the toroidal field alone will increase the power threshold, since it reverses the toroidal flow, now resulting in a negative toroidal angular momentum input, and also reverses E_v (and thus E_r).
- Reversal of all fields, but still remaining in LSN, has no effect on the flows but reverses E_v, thus increasing the threshold.
- Keeping the currents and fields in the 'normal' direction but switching to an USN topology will increase the threshold, since the momentum input reverses (upper, positive part of the toroidal flow gets damped), and E_v, although still positive, reverses direction with respect to the X-point.
- Note that these changes all lead to reversal of the ∇B-drift direction with respect to the location of the X-point, which is known to increase the power threshold by about a factor of two [13].

A more quantitative look at the effects of the Pfirsch–Schlüter-generated radial electric field in equation (15) on the L–H transition power threshold is underway and will be presented in a future work.

5. Summary

We demonstrated a dynamical mechanism for driving edge flows in toroidal devices. A residual vertical electric field that results from a balance between collisional effects and ∇B-dependent drifts at the plasma edge drives a toroidally outward flow within the separatrix, with an accompanying return flow outside, mainly due to parallel pressure gradients. The direction of the poloidal component of these flows is independent of the field direction; however, there is an anti-symmetric toroidal component that reverses with the toroidal field. In a symmetric system, there is no net toroidal angular momentum associated with these flows. Field and boundary asymmetries, however, can lead to a net momentum input by preferentially damping part of this anti-symmetric toroidal flow, thus providing an intrinsic momentum source. This effect and the expected reversal of the residual electric field E_v with the toroidal field have the right symmetry properties to account for the increased power threshold for the L–H transition when the ∇B-drift points away from the active X-point.

Appendix A. Symmetry under reversal of the toroidal field

In an axisymmetric system, 'simultaneous reversal of toroidal magnetic field and poloidal plasma flow' [14], interpreted as $B_\phi \to -B_\phi, v_R \to -v_R, v_Z \to -v_Z$ (in an (R, ϕ, Z) cylindrical coordinate system), was shown to be *not* a symmetry of either the fluid or kinetic time-dependent plasma models [15]. In the same reference [15], the time-*in*dependent MHD and Vlasov models were shown to be invariant under this set of transformations, but the relevance of this partial symmetry in predicting the behaviour of flows in a tokamak was questioned at some length.

There is a symmetry transformation $B_\phi \to -B_\phi$, $Z \to -Z, v_Z \to -v_Z$, i.e. with an additional coordinate reflection $Z \to -Z$, that leaves the time-dependent kinetic models invariant, if one makes the additional assumption of up–down symmetry [16]. However, as shown in [15], this transformation first flips the tokamak up-side down ($Z \to -Z$), thus reversing the toroidal field B_ϕ, toroidal current I_ϕ, toroidal and poloidal flows, then reverses back the toroidal field and poloidal flow, leaving the toroidal current and toroidal flow in a reversed state. Therefore, this transformation does not represent 'simultaneous reversal of toroidal magnetic field and poloidal plasma flow' but is equivalent to the well-known symmetry $I_\phi \to -I_\phi, v_\phi \to -v_\phi$ [16], specialized to up–down symmetric tokamaks.

Finally, for the flows discussed in this work, symmetry under the transformation $B_\phi \to -B_\phi, v_\phi \to -v_\phi$ follows simply from the physics behind them, as shown in sections 1 and 2. That it is a proper symmetry of the time-dependent MHD equations was shown in [5, 6], and reiterated in [15]. In addition, since the flows within the separatrix discussed in this work are essentially $\boldsymbol{E}\times\boldsymbol{B}$ flows, a characteristic of MHD, their discussion within an MHD framework seems appropriate.

Appendix B. Sign of the function $f(\psi, \theta)$ in equation (15)

In section 2, sign of the radial electric field was shown to depend on the purely geometric factor $f(\psi, \theta)$ defined as

$$f(\psi,\theta) \equiv \int_0^\theta R^2\, \mathrm{d}\tilde{\theta} - \theta\overline{R^2}, \quad \overline{R^2} \equiv \frac{1}{2\pi}\oint R^2\, \mathrm{d}\tilde{\theta}.$$

Here we show that f is positive (negative) in the upper (lower) half planes under quite general conditions.

Assume that the plasma boundary is parametrized by $R = R(\psi = \psi_{\rm sep}; \theta)$, $Z = (\psi = \psi_{\rm sep}; \theta)$, and for convenience let $f(\theta) \equiv f(\psi = \psi_{\rm sep}; \theta)$. It is clear that $f(-\theta) = -f(\theta)$; thus $f(0) = f(\pi) = 0$. Assume also that $R_{\rm max} = R(\psi_{\rm sep}; \theta = 0)$, and $R_{\rm min} = R(\psi_{\rm sep}; \theta = \pi)$. Then $\partial f/\partial\theta = R^2 - \overline{R^2}$ is positive at $\theta = 0$ and negative at $\theta = \pi$. Thus, $\partial f/\partial\theta$ has to vanish at least at one point in the interval $(0, \pi)$. But if $R(\psi_{sep}; \theta)$ is a monotonically decreasing function of θ in this interval (a reasonable assumption), then $\partial f/\partial\theta$ will vanish exactly at one point only. Thus, $f(\theta) \geqslant 0$ in $[0, \pi]$. $f(\theta) \leqslant 0$ in $[\pi, 2\pi]$ follows from the odd symmetry of $f(\theta)$.

Acknowledgments

This research was supported by the Office of Fusion Energy Science of the US Department of Energy under Grant DE-FG02-04ER54742.

References

[1] Asakura N., Sakurai S., Itami K., Naito O., Tagenaga H., Higashijima S., Koide Y., Sakamoto Y., Kubo H. and Porter G.D. 2003 *J. Nucl. Mater.* **313** 820
[2] LaBombard B. *et al* and the Alcator Group 2004 *Nucl. Fusion* **44** 1047
[3] Pitts R.A. *et al* 2005 *J. Nucl. Mater.* **337** 146
[4] Simakov A.N., Catto P.J., LaBombard B. and Glasser A.H. 2008 Magnetic topology effects on Alcator C-Mod scrape-off layer flow *Plasma Phys. Control. Fusion* **50** 105010
[5] Aydemir A.Y. 2007 Shear flows at the tokamak edge and their interaction with edge-localized modes *Phys. Plasmas* **14** 056118
[6] Aydemir A.Y. 2007 Shear flows at the tokamak edge and their role in core rotation and the L–H transition *Phys. Rev. Lett.* **98** 225002
[7] Kamp L.P. and Montgomery D.C. 2003 *Phys. Plasmas* **10** 157
[8] Kamp L.P. and Montgomery D.C. 2004 *J. Plasma Phys.* **70** 113
[9] Jardin S., Sovinec C., Breslau J., Ferraro N., Hudson S., King J., Kruger S., Ramos J. and Schnack D. 2008 *Proc. 22th IAEA Fusion Energy Conf. (Vienna, Austria, 2008)* (Vienna: IAEA) CD-ROM file TH/P9-29 and http://www-naweb.iaea.org/napc/physics/FEC/FEC2008/html/index.htm
[10] Takuzika T., Shimizu K., Hayashi N., Hosokawa M. and Yagi M. 2009 Two-dimensional full particle simulation of the flow patterns in the scrape-off layer plasma for upper- and lower-null point divertor configurations in tokamaks *Nucl. Fusion* submitted
[11] LaBombard B. *et al* and Alcator C-Mod Team 2008 *Phys. Plasmas* **15** 056106
[12] Shaing K.C. and Crume E.C. 1989 *Phys. Rev. Lett.* **63** 2369
[13] Ryter F. and the H-Mode Database Working Group 1996 *Nucl. Fusion* **36** 1217
[14] Simakov A.N. and Catto P.J. 2009 Response to comment on magnetic topology effects on Alcator C-Mod scrape-off layer flow *Plasma Phys. Control. Fusion* **51** 048002
[15] Aydemir A.Y. 2009 Comment on magnetic topology effects on Alcator C-Mod scrape-off layer flow *Plasma Phys. Control. Fusion* **51** 048001
[16] Cohen R.H. and Ryutov D.D. 2001 *Phys. Plasmas* **8** 1451